Segmentation of echocardiographic images with Markov random fields

Isabelle Herlin, Dominique Béréziat, Gérard Giraudon, Catherine Nguyen, Christine Graffigne

INRIA
INSTITUT NATIONAL DE RECHERCHE EN INFORMATIQUE ET EN AUTOMATIQUE

Segmentation of echocardiographic images with Markov random fields

I.L. HERLIN, D. BÉRÉZIAT, G. GIRAUDON, C. NGUYEN, C. GRAFFIGNE

N° 2424

Décembre 1994

PROGRAMME 4

ISSN 0249-6399

ROCQUENCOURT

Segmentation of echocardiographic images with Markov random fields

I.L. HERLIN, D. BÉRÉZIAT, G. GIRAUDON, C. NGUYEN, C. GRAFFIGNE

Programme 4 — Robotique, image et vision

Projet MASDA

Rapport de recherche n° 2424 — Décembre 1994 — 18 pages

Abstract: The aim of this work is to track specific anatomical structures in temporal sequences of echocardiographic images. Ultrasound images are available in two broad data types: raw or video data. Different stochastic processes using different kind of information are compared on the basis of these two data types.

We explain the selection of a particular model w.r.t. the type of data, and describe the relevant properties that must be taken into account to obtain the best possible results.

The models are expressed within a Markov random field framework and we also discuss parameter estimation and energy minimization for the different models.

Key-words: Segmentation, Markov Random Field, Stochastic Process, Medical Image, Ultrasound.

(Résumé : tsvp)

Unité de recherche INRIA Rocquencourt

Domaine de Voluceau, Rocquencourt, BP 105, 78153 LE CHESNAY Cedex (France)

Segmentation d'images échocardiographiques par champs de Markov

Résumé : Le but de ce travail est l'étude du suivi de structures anatomiques particulières dans des séquences temporelles d'images échocardiographiques. Les images ultrasonores sont en fait disponibles selon deux types de format : les données ultrason originales ou les données vidéo. Cet article présente donc différents processus stochastiques destinés à résoudre le problème de la segmentation spatio-temporelle sur les deux types de données disponibles.

Nous explicitons les informations images nécessaires pour obtenir les meilleurs résultats possibles de segmentation spatio-temporelle et précisons un modèle satisfaisant pour ces deux types de données.

Les modèles présentés dans cet article sont exprimés dans un formalisme de champ markovien aléatoire et nous présentons une discussion sur le choix des valeurs de paramètres, sur la robustesse des algorithmes et sur la technique d'optimisation utilisée.

Mots-clé : Segmentation, Champ de Markov Aléatoire, Processus Stochastique, Imagerie médicale, Ultrason.

1 Introduction

1.1 Motivation and objectives

In [6] a model of segmentation for cardiac cavities in ultrasound images has been presented. This model is operating with video data and supposes that grey level values of pixels inside the cavity follow a normal law with constant mean and standard deviation. It supposes also that cavity's boundary includes a lot of points having a high gradient norm value, and that the boundary is smooth. Section 2 will explain how these properties are mathematically translated; why this model is sometimes inaccurate; and why we found necessary to define a spatio-temporal model [7]. This new model includes temporal properties in three different ways: in the first place we include a temporal neighborhood in the Markov random field model; secondly we use, inside the segmentation process, the result obtained from the previous image of the sequence; and thirdly we use a geometrical constraint on the cavity's center of mass. In section 3, we analyze the limitations of these models and study their accuracy.

Finally, in section 4, we will present a new spatio-temporal model running either on video data or raw data. We translate the three previous spatial properties in a different way to avoid the segmentation problems discussed in section 2. In the same manner, we define differently the temporal constraints in order to take two different types of temporal motion into consideration: the cardiac boundaries are moving slowly during the cardiac cycle; the mitral valves are moving very fast.

A study of the stability of our segmentation process w.r.t. the iteration count of the optimization is presented. We also show how the algorithm operates on raw data.

Results are presented all along the sections of this paper, as are also described some cases of inaccuracy and improvements of the segmentation process.

1.2 Previous work

Gibbs fields or Markov fields are standard probabilistic tools in statistical mechanics. The link between Gibb's laws and two dimensional Markov properties goes back to a famous theorem of Hammersley. However applications of these notions to images viewed as two-

dimensional arrays is much more recent, and a major step in that direction was D. and S. Geman's paper on image restoration [4].

The aim of the work presented here is non supervised segmentation based on a region growing algorithm [1], [9]. Our paper is concerned with a special case of a region growing algorithm segmenting a cardiac cavity on ultrasound images.

We are also concerned with direct use of ultrasonic raw data, before transformation to cartesian video data. To our knowledge very few studies are done directly on these data [5, 8], but we have verified that the quality of edges and extracted features can be enhanced on these images.

2 The spatial model

This model is extensively described in [6]. In this section we only summarize its properties, show how they are mathematically translated and also illustrate its limitations with sample images on which it leads to inaccurate segmentation. Fig. 1 displays the echocardiographic data and the cavity of interest. These data were obtained on a VINGMED echograph from Henri Mondor Hospital, France (Thanks to Gabriel Pelle).

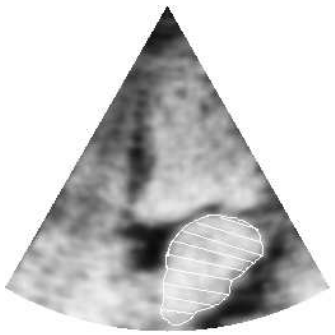

Figure 1: Echocardiographic video image and the studied cavity.

We first define the following sets and variables:

- S denotes the set of pixels of the image;
- $\Gamma = \{0, \ldots, 255\}^{|S|}, \Omega = \{-1, 1\}^{|S|}$;

- $Im = (Im_s)_{s \in S}$ is a random variable defining the grey level values of the pixels. Its realization is $im = (im_s)_{s \in S} \in \Gamma$;
- $G = (G_s)_{s \in S}$ encodes the norm of spatial gradient, $g = (g_s)_{s \in S} \in \Gamma$ and is obtained by Deriche's algorithm [3];
- $E = (E_s)_{s \in S}$ defines the edge process, $e = (e_s)_{s \in S} \in \Omega; e_s = 1 \iff s$ is an edge point;
- $X = (X_s)_{s \in S}$ defines the segmentation process: $x = (x_s)_{s \in S} \in \Omega$ and $x_s = 1 \iff s$ is inside the cavity; we denote by $C(x)$ the set of pixels inside this cavity;
- ν_s is the neighborhood of s;
- $y = (im, g, e)$ denotes the observation, as a result of process $Y = (Im, G, E)$; x^0 is an initial segmentation for the cavity, used at the initialization of the optimization process;
- lastly, P is the conditional probability of X knowing Y. $P(X/Y = y) = \exp(-U(X/Y = y))/Z_y$ in the mathematical framework of Gibbs distribution and Markov random fields [4].

It is important to explain how visual properties of the echocardiographic sequence are mathematically translated. Indeed, our choice is not the only possible one, and it might have to be revised each time results are considered as insufficient or inaccurate:

- the grey level values of the pixels inside the cavity are homogeneous. This property is translated into the following assumption: $\forall s \in C(x), im_s \sim \mathcal{N}(\mu, \sigma^2)$: the grey level value of each pixel of the cavity follows a normal law of constant mean μ and constant standard deviation σ.

  This property defines a first term, U_1, of the energy function, which is minimized during the optimization process:

$$U_1(x, y) = \sum_{x \in C(x)} \left(\left(\frac{im_s - \mu}{\sigma} \right)^2 - f(y) \right), \tag{1}$$

  $f(y)$ being a local threshold.

- $f(y)$ may be constant, equal to the value T, where T is defined by the normal law table for a chosen percentage (95% or 99%).
- $f(y)$ may also be variable, incorporating the second property: the initial boundary of the cavity is attracted by high gradient norm values and the growing process must stop at the edge points:

$$f(y) = T + \beta g_s(1 - e_s), \tag{2}$$

β being a parameter with positive value.

The value of $U_1(x, y)$ is then decreasing if points with high gradient norm value are labelled as being inside the cavity.

- The third visual property concerns cavity's smoothness and boundary's smoothness. This property is expressed in an Ising model: the probability that a pixel is labelled 1, or -1, becomes higher if points in the neighborhood possess the same label. This is expressed by a second term of the energy function:

$$U_2(x) = -\alpha \sum_s x_s \left(\sum_{t \in \nu_s} x_t \right), \tag{3}$$

α being a positive parameter.

We suppose that $X = (X_s)_{s \in S}$ is a random field, defined on Ω, with a Gibbs distribution associated to the neighborhood system $\{\nu_s\}$:

$$\forall x \in \Omega, P(X = x) = \Pi(x) = \frac{e^{-U_2(x)}}{Z},$$

where:

$$U_2(x) = -\alpha \sum_{s \in S} \sum_{t \in \nu_s} x_s x_t,$$

this is an a priori probability distribution law for X;

$$Z = \sum_{x \in \Omega} e^{-U_2(x)}$$

is called the partition function.

We suppose also that $Y = (Y_s)_{s \in S}$ is a random field on $\Delta = \Gamma \times \Gamma \times \Omega$, and that its conditional distribution, knowing $X = x$, is:

$$\forall y \in \Delta \qquad P(Y = y/X = x) = \Pi(y/x) = \frac{e^{-U_1(y/x)}}{Z_x},$$

with

$$U_1(y/x) = U_1(x, y) = \sum_{s \in C(x)} \left[\left(\frac{im_s - \mu}{\sigma} \right)^2 - f(y) \right], \tag{4}$$

and

$$Z_x = \sum_{y \in \Delta} e^{-U_1(x,y)} \ .$$

From Bayes theorem, we get:

$$\Pi(x/y) = P(X = x/Y = y) \ \alpha \ P(Y = y/X = x) * P(X = x) \ \alpha \ \exp -\{U_1(x, y) + U_2(x)\},$$

where α means "proportional". We obtain an a posteriori distribution of X, called $\Pi(x/y)$, defined on Ω by:

$$\forall x \in \Omega \qquad \Pi(x/y) = \frac{e^{-U(x/y)}}{Z_y}, \tag{5}$$

with

$$\begin{aligned} U(x/y) &= U_1(x, y) + U_2(x) \\ &= \sum_{s \in C(x)} \left[\left(\frac{im_s - \mu}{\sigma} \right)^2 - f(y) \right] - \alpha \sum_{s \in S} \sum_{t \in \nu_s} x_s x_t, \end{aligned} \tag{6}$$

and $Z_y = \sum_{x \in \Omega} e^{-U(x/y)}$.

Knowing a realization y of the random field Y, we are looking for the realization x of the random field X, which maximizes the a posteriori distribution of X knowing $Y = y$. In other words, we seek:

$$x^* = \arg \left(\max_{x \in \Omega} (\Pi(x/y)) \right).$$

x^* is called **M**aximum **A** **P**osteriori (**MAP**) estimator of $\Pi(x/y)$.

Moreover $U(x/y)$ can be written:

$$U(x/y) = \sum_{c \in C} U_c(x/y), \tag{7}$$

where C is the set of singles $\{s\}$ and pairs $\{s, t\}$, with $t \in \nu_s$, and $U_c(x/y)$ is defined by:

- $U_{\{s\}}(x/y) = \left[\left(\frac{im_s - \mu}{\sigma}\right)^2 - T - \beta g_s(1 - c_s)\right]$, if $s \in C(x)$,
- $U_{\{s,t\}}(x/y) = -\alpha x_s x_t$.

$\Pi(x/y)$ is a Gibbs distribution associated with $U(x/y)$ and C.

Hammersley–Clifford's theorem demonstrates the equivalence between Markov random fields and Gibbs distributions. Computation of the exact minimum of the energy function or the exact maximum of Gibb's distribution is time consuming, so we use approximations to get the cavity's boundary. Because this segmentation process uses only two labels, 1 and -1 (inside and outside the cavity), and since the cavity is connected, we make the choice of an **I**terated **C**onditional **M**ode method (**ICM**) [2], which does not produce a global minimum of the energy function but is a fast deterministic algorithm: knowing an initial segmentation x_0, we maximize iteratively, at each pixel s of the image, the local conditional probability $\Pi(x_s/x_{\nu_s}, y)$ of the label value x_s knowing the label values in the neighborhood x_{ν_s} and the observation y:

$$\hat{x}_s = \arg\left(\max_{\lambda_s \in \{-1,1\}} (\Pi(\lambda_s/x_{\nu_s}, y))\right)$$

We must then compare $\Pi(1/x_{\nu_s}, y)$ and $\Pi(-1/x_{\nu_s}, y)$ or, equivalently, compare $\left(\frac{im_s - \mu}{\sigma}\right)^2$ with a local threshold

$$f(y) + 2\alpha \sum_{t \in \nu_s} x_t = T + \beta g_s(1 - c_s) + 2\alpha \sum_{t \in \nu_s} x_t. \tag{8}$$

This model contains a number of parameters: μ, σ, T, α and β. We will now explain how we determine or constrain their values:

- μ and σ are the maximum likehood estimators for the gaussian law $\mathcal{N}(\mu, \sigma^2)$ of the grey level value inside the cavity,
- T is a classical gaussian threshold chosen such that: $\forall s \in C(x^0)$ (interior of the initialization of the cavity) $\left(\frac{im_s - \mu}{\sigma}\right)^2 < T$,
- α is defined as $\alpha = \sup\left(\alpha', \frac{T}{8}\right)$ where:

– α' verifies:

$$\forall s \in S, \text{ satisfying } -2 \leq \sum_{t \in \nu_s} x_t^0 \leq 2,$$

(s is a pixel near the boundary of the initialization of the cavity), we have:

$$\left(\frac{im_s - \mu}{\sigma}\right)^2 \leq T + 2\alpha' \sum_{t \in \nu_s} x_t,$$

in order to obtain a growing process starting with the initialization;

– $\frac{T}{8}$ corresponds to the following property:

$$P(x_s = 1 / \sum_{t \in \nu_s} x_t = -4) < P(x_s = -1 / \sum_{t \in \nu_s} x_t = -4),$$

that must be verified for smoothness constraint.

- β is estimated with the following principle: in a first phase of the segmentation, the model is used without any gradient property ($\beta = 0$). Then, starting from the initialization x^0, we obtain a first result x^1. β is estimated on the boundary of $C(x^1)$ using the following property:

$$\forall s \in S, \text{ satisfying } 0 \leq \sum_{t \in \nu_s} x_t \leq 2,$$

(s is a pixel near the boundary of $C(x^1)$ and inside $C(x^1)$) we require:

$$\left(\frac{im_s - \mu}{\sigma}\right)^2 \leq T + \beta g_s(1 - c_s) + 2\alpha \sum_{t \in \nu_s} x_t,$$

that is to say that the local threshold is increasing as pixels with high gradient norm values are included inside the cavity during the growing process.

But we found this algorithm inadequate due to the following problems:

- the segmentation escapes outside of the cavity when the mitral valve is open (see Fig. 2);
- the result of segmentation is not stable as the number of iterations of the ICM increases (see Fig. 3).

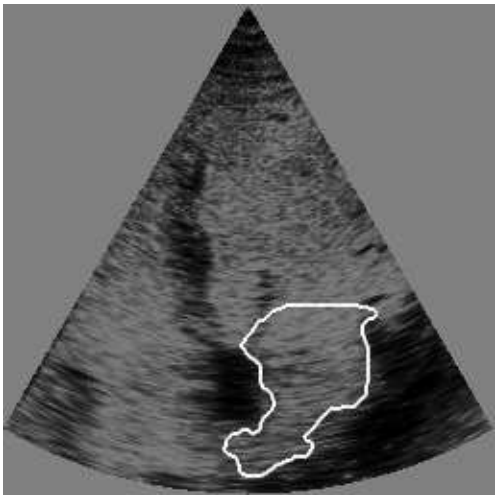

Figure 2: Mitral valves are opened: inaccuracy of segmentation

Figure 3: Results of segmentation with 5, 10 and 20 **ICM** (left to right).

To avoid the first problem, we try to add temporal properties and begin with a first simple solution by adding a temporal neighborhood into the Ising model. The new neighborhood system is $\nu'_s = \{\nu_s, s_{n-1}, s_{n+1}\}$ where ν_s is the spatial neighborhood and s_{n-1}, s_{n+1} are the pixels, at same position than s, on the previous image and on the next image of the sequence (n is the count of the studied image). The probability that a point is labelled 1, inside the cavity (or -1, outside the cavity), becomes higher if the point has the same label on the previous image or on the next image.

However, this simple constraint is very strong and the segmentation result becomes too stable from an image to the next, and some modifications of the cavity are lost. On another hand, this temporal constraint is able to solve the problem of the opening of the mitral valve as shown on Fig. 4: the result of segmentation does escape from the cavity.

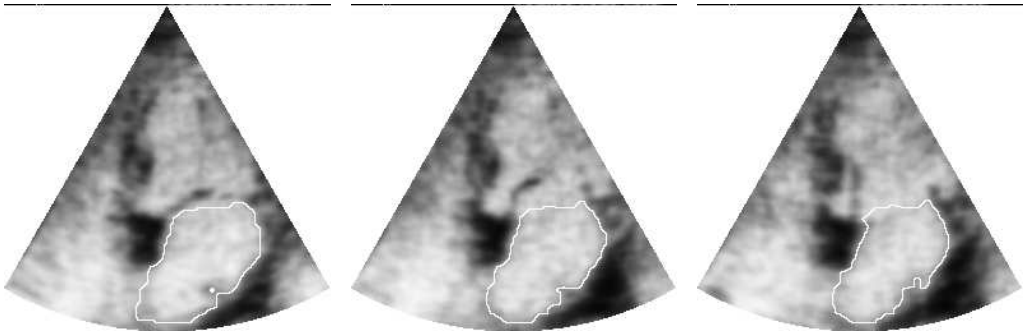

Figure 4: Results of segmentation on three consecutive images of the sequence.

We concluded that temporal information has to be used in a different way. We define a more precise spatio-temporal model that is presented and discussed in the following section.

3 The spatio-temporal model

This model, published in [7], is a temporal extension of the previous one.

Firstly, we have to be more specific about grey level values. So we transform the first term in the energy function in the following way:

$$U_1(x,y) = \sum_{s \in C(x)} \left(\left(\frac{im_s - \mu_s}{\sigma} \right)^2 - f(y) \right), \tag{9}$$

so that it admits a local mean μ_s.

This local mean must express the fact that the grey level values become lower (i.e. darker) in the region of the cardiac muscle, where the gradient norm has high value. We then define:

- $f(y) = T$, this threshold has a constant value corresponding to the normal law model;
- $\mu_s = \mu_0 + k g_s (1 - c_s)$, k being negative, the value of μ_s is then decreasing from the center to the cavity's boundary.

As a matter of fact, these different mathematical formulations give the same results. Only the necessary number of ICM iterations becomes lower if one uses a local mean in which the gradient norm property is taken into account.

We then define new temporal properties to express the temporal regularity of the cavity over the sequence. This new model makes use of a reference cavity called C_{ref} obtained by the result of the segmentation process on the previous image of the sequence (on the first image C_{ref} may be defined interactively or may be obtained by the spatial model). This cavity is used in two ways:

- for a point labelled 1 on the reference cavity, the probability that it keeps the same label becomes higher. This is why we add a new term to the energy function:

  $$-\alpha \sum_{s \in S} x_r r_s,$$

  where r_s is the label of pixel s on the reference image; $r_s = 1$ if the point is labelled as inside the cavity of interest and $r_s = -1$ outside this cavity.

- We also suppose that the position of the center of mass is not varying from an image to the next. This global constraint cannot be easily translated into a Markov random field formulation and we approximate it by adding an isotropic constraint on the distance

between each pixel of the cavity and the center of mass of the reference cavity (its coordinates are $(k_{\text{ref}}, l_{\text{ref}})$):

$$\gamma \sum_{s \in C(x)} [(k_s - k_{\text{ref}})^2 + (l_s - l_{\text{ref}})^2 - dm^2],$$

where (k_s, l_s) are the coordinates of s.

Our last energy term prevents a growing of the segmentation process in one particular direction. It avoids a penetration inside the other cavity if the mitral valve is open.

This new model includes four parameters: $k_{\text{ref}}, l_{\text{ref}}, dm$ and γ. They are defined by:

- k_{ref} and l_{ref} are the coordinates of the reference cavity C_{ref} (in the previous image of the sequence),
- dm is the maximal distance between the center of mass and the mitral valve on the reference cavity, this is the maximal distance that we will admit for the segmentation process,
- γ is estimated by: $\forall s \in S$, satisfying $(k_s - k_{\text{ref}})^2 + (l_s - l_{\text{ref}})^2 = 1.1dm^2$, we have

$$\gamma > \frac{T + \alpha \left(\sum_{t \in \nu_s} x_t + r_s\right) - \left(\frac{im_s - \mu}{\sigma}\right)^2}{0.1dm^2}$$

to put a penalty on pixels outside the circle with center $(k_{\text{ref}}, l_{\text{ref}})$ and radius dm.

We have used this model on the video images to get the following conclusions:

- The use of a reference cavity is restrictive. Indeed let dm be the maximal distance on the reference cavity between the mitral valve and the center of mass. The model makes the assumption that this maximal distance will be less than 1.1 dm on the next image of the sequence. This is quite an important temporal smoothness assumption, which depends on the temporal resolution of the sequence. It is more or less difficult to ensure.
- The temporal constraint is isotropic: it does not allow for the segmentation to grow inside the other cavity (because of the choice of dm) but it does not prevent penetration in the other parts of the boundary, which are less far from the center of mass than dm: if pixels are nearer than dm the label 1 is prefered. This is shown on Fig. 5.

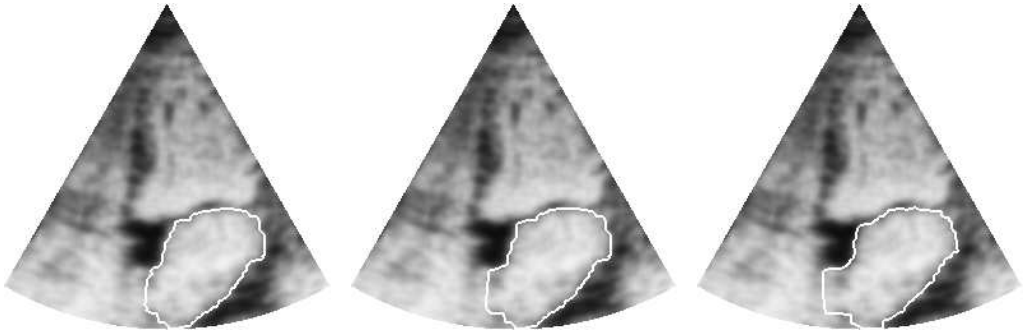

Figure 5: Effect of the isotropic constraint after 5, 10 or 20 ICM, left to right.

4 A new spatio-temporal model on raw data

After comparison between different models, we conclude that the properties which are important for the segmentation process are:

- homogeneity,
- smoothness,
- spatial gradient,
- temporal information.

We have discussed why the previous modelisations on temporal information are inaccurate:

- spatio-temporal neighborhoods includes information that is too local,
- the center of gravity property is a constraint that is too important and also includes an isotropic property.

In fact we need a temporal regularity constraint in the region of the mitral valve because it is varying very fast.

In this region we have the following properties:

- the value of the spatial gradient (g_s) is low,

- the value of the temporal gradient (gt_s) is high.

These properties are expressed by the energy function:

$$U(x/y) = \sum_{s \in C(x)} \left[\left(\frac{im_s - \mu_s}{\sigma} \right)^2 - T \right] - \alpha \sum_{<s,t>} x_s x_t + \delta \sum_{s \in S} (\phi_c(g_s) * \Psi_{c'}(gt_s)), \qquad (10)$$

where ϕ_c and $\Psi_{c'}$ are two functions in $C^1(\mathbb{R}, [0,1])$ satisfying:

- $\phi_c(0) = 1; \phi_c(c) = 1/2;$
- $\lim_{x \to \infty} \phi_c(x) = 0;$
- $\Psi_{c'}(0) = 0; \Psi_{c'}(c) = 1/2;$
- $\lim_{x \to \infty} \Psi_{c'}(x) = 1.$

Graphs of these functions are shown on Fig. 6.

ϕ_c is a thresholding function of the high values of the spatial gradient and $\Psi_{c'}$ is a thresholding function of the low values of the temporal gradient.

With such a modelisation a point is labelled as inside the cavity if $\left(\frac{im_s - \mu_s}{\sigma} \right)^2 \leq t_{\text{loc}}$, with:

$$t_{\text{loc}} = T + 2\alpha \sum_{t \in \nu_s} x_t - 2\delta \phi_c(g_s) * \Psi_{c'}(gt_s) \ . \qquad (11)$$

Now t_{loc} becomes very low in the region of the mitral valve and the growing process will stop because we impose $x_s = -1$ (outside the cavity) when reaching this region.

The thresholding functions include a weighting coefficient δ that must verify the following property: if $(\phi_c(g_s) \simeq 1)$ and $(\Psi_{c'}(gt_s) \simeq 1)$ (i.e. low spatial gradient and high temporal gradient) we will ensure that $\left(\frac{im_s - \mu_s}{\sigma} \right)^2 > t_{\text{loc}}$. δ must verify:

$$\delta > \frac{T + 2\alpha \sum_{t \in \nu_s} x_t - \left(\frac{im_s - \mu_s}{\sigma} \right)^2}{2\phi_c(g_s) * \Psi_{c'}(gt_s)} \ . \qquad (12)$$

δ is estimated with the result of the spatial model on the first image of the sequence.

We studied this model with the following choices for ϕ_c and $\Psi_{c'}$:

- $\phi_c(x) = \frac{1 - F(x/c)}{2}$,

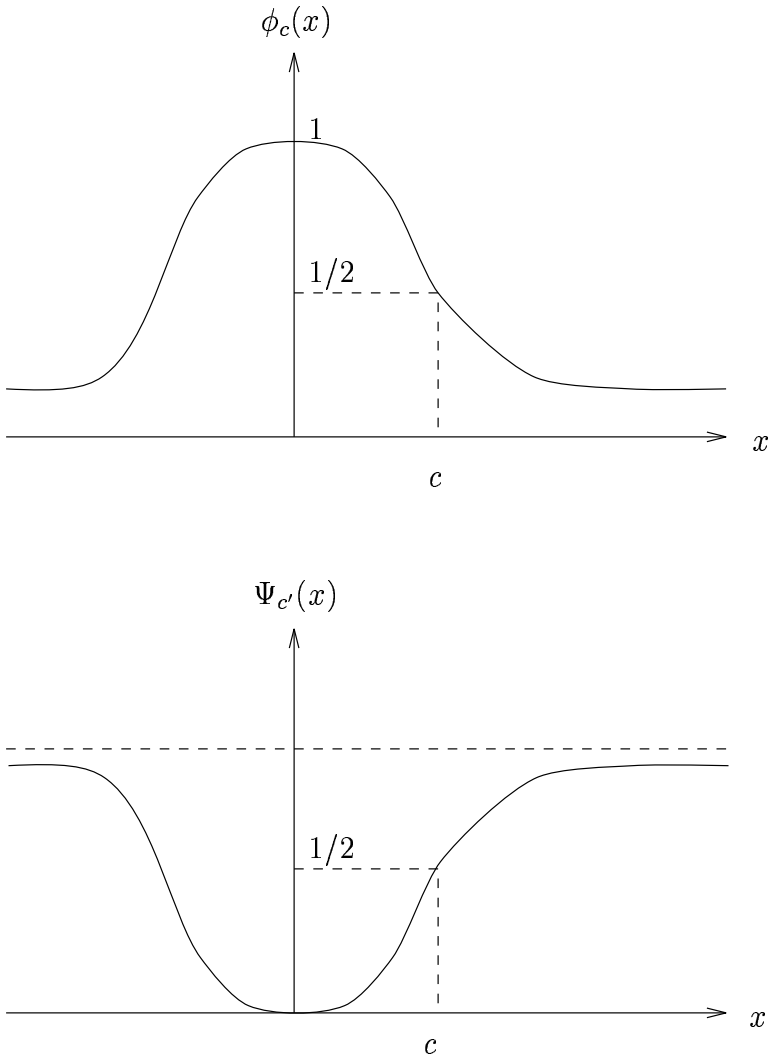

Figure 6: Graphs of ϕ_c and $\Psi_{c'}$.

- $\Psi_{c'}(x) = \frac{1+F(x/c')}{2}$,
- $F(x) = \frac{1-x^a}{1+x^a}, a > 1$,
- c is the mean of the norm of the spatial gradient on the whole image,
- c' is the mean of the norm of the temporal gradient.

The value of a allows to adjust the slope of the functions. We choose $a = 2$.

With these choices, we tested the model on video data and on raw polar data and concluded that:

- The results obtained with this model are better, even if the mitral valve is open, as is shown on Fig. 7 (left).
- Moreover, the result are more stable regarding to the iteration count of the ICM algorithm. This is illustrated on Fig. 7 where the result with 5, 10 or 20 iterations of ICM are displayed from left to right. On the right image, we can observe penetrations in the borders of the mitral valve only because the segmentation algorithm works with pixels with high gradient norm values inside the cavity.

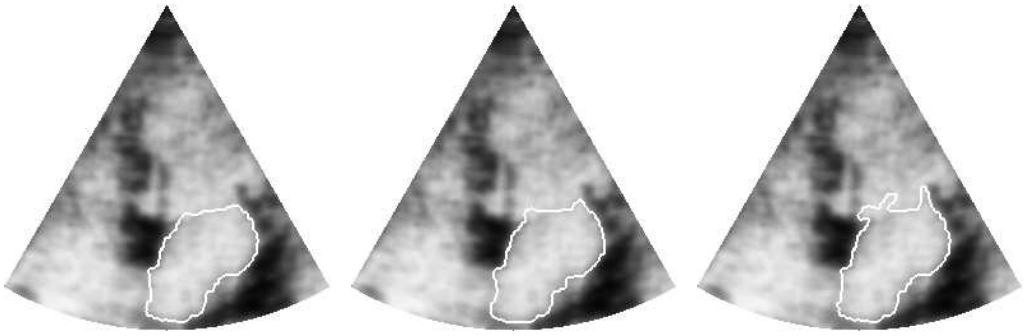

Figure 7: Results of the model when the mitral valve is opened with 5, 10 and 20 ICM from left to right.

We tested our model on original raw data obtained from the echograph before conversion into cartesian coordinates (the conversion into cartesian coordinates is used by the physician

which looks at the data displayed on a video device). The size of these images is very low: 64 lines (each for one ultrasound ray) of 512 pixels.

Fig. 8 displays one of these images and the studied cavity. A first question involves the scanning process of the image. We used a classical line by line scanning illustrated on Fig. 9. Since the shape of the cavity is elongated horizontally, it is worth studying these polar images after a 90° rotation. Figs. 10, 11, 12 display the results of this model on three different polar images.

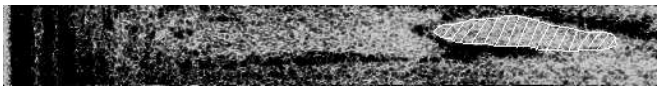

Figure 8: Ultrasound raw data and the studied cavity.

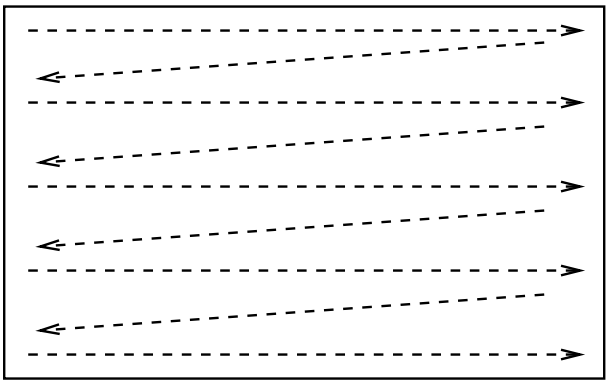

Figure 9: Scanning of the image.

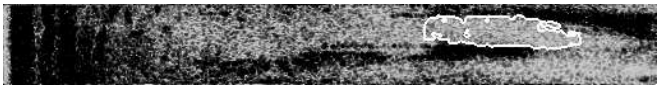

Figure 10: Result on image 1.

Figure 11: Result on image 2.

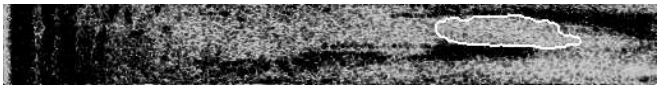

Figure 12: Result on image 11.

5 Conclusion

In this paper, we have compared different stochastic processes for segmentation, running either on video data or original polar data. We have made the conclusion that the following properties must be taken into account for segmentation:

- homogeneity of grey level values: this property must be expressed with a local mean to ensure acceptable computation time;
- attraction of the boundary of the cavity (during the region growing process) by the pixels with high gradient norm values; this property is included inside the local mean formulation;
- spatial smoothness of the result, obtained with the help of an Ising model for example;
- temporal regularity of the segmentation: we have seen that making use of a local temporal neighborhood is too restrictive and that a global geometric constraint on isotropy is not valid for raw data; our solution makes use of temporal gradient: this is a local constraint that takes into account all the images for a recursive implementation.

We have presented our results for different models expressing different properties, illustrating problems that may appear and we made the choice of a particular model operating either on raw or video data.

References

[1] R. Azencott and C. Graffigne. Non supervised segmentation using multi-level markov random fields. In *Proceedings of the 11th International Conference on Pattern Recognition*, August 30-September 3 1992.

[2] J. Besag. On the statistical analysis of dirty pictures. *Journal of Royal Statistical Society*, 48, 1986.

[3] R. Deriche. Using Canny's criteria to derive a recursively implemented optimal edge detector. *International Journal of Computer Vision*, 1 (2), May 1987.

[4] S. Geman and D. Geman. Stochastic relaxation, Gibbs distribution and the Bayesian restoration of images. *IEEE Transactions on Pattern Analysis and Machine Intelligence*, 6:712–741, 1984.

[5] I. Herlin and N. Ayache. Features extraction and analysis methods for sequences of ultrasound images. In *Proceedings of the Second European Conference on Computer Vision 1992*, May 1992.

[6] I. Herlin, C. Nguyen, and C. Graffigne. Stochastic segmentation of ultrasound images. In *Proceedings of the 11th International Conference on Pattern Recognition*, August 30-September 3 1992.

[7] I. L. Herlin and G. Giraudon. Use of temporal information in a segmentation algorithm of ultrasound images. In *Proceedings of the conference on Computer Vision and Pattern Recognition*, New York, U.S.A., 15-17 June 1993.

[8] T. Taxt, A. Lundervold, and B. Angelsen. Noise reduction and segmentation in time-varying ultrasound images. In *10th International Conference on Pattern Recognition*, Atlantic City, New Jersey, USA, June 1990.

[9] S.W. Zucker. Region growing: Childhood and adolescence. *Computer Graphics and Image Processing*, (5):382–399, 1976.

Unité de recherche INRIA Lorraine, Technopôle de Nancy-Brabois, Campus scientifique,
615 rue du Jardin Botanique, BP 101, 54600 VILLERS LÈS NANCY
Unité de recherche INRIA Rennes, Irisa, Campus universitaire de Beaulieu, 35042 RENNES Cedex
Unité de recherche INRIA Rhône-Alpes, 46 avenue Félix Viallet, 38031 GRENOBLE Cedex 1
Unité de recherche INRIA Rocquencourt, Domaine de Voluceau, Rocquencourt, BP 105, 78153 LE CHESNAY Cedex
Unité de recherche INRIA Sophia-Antipolis, 2004 route des Lucioles, BP 93, 06902 SOPHIA-ANTIPOLIS Cedex

Éditeur

INRIA, Domaine de Voluceau, Rocquencourt, BP 105, 78153 LE CHESNAY Cedex (France)

ISSN 0249-6399